Far-field brittle deformation record in the eastern Paris Basin (France)

Thomas Blaise, Sid Ahmed Ali Khoudja, Cédric Carpentier, Benjamin Brigaud, Yves Missenard, Xavier Mangenot, Philippe Boulvais, Philippe Landrein, Jean Cochard

Far-field brittle deformation record in the eastern Paris Basin (France)

***Original Article – Special issue** "Faults and fractures in rocks: mechanics, occurrence, dating, stress history and fluid flow"*

Thomas Blaise*[1], Sid Ahmed Ali Khoudja[1], Cédric Carpentier[2], Benjamin Brigaud[1], Yves Missenard[1], Xavier Mangenot[3], Philippe Boulvais[4], Philippe Landrein[5], Jean Cochard[5]

[1] Université Paris-Saclay, CNRS, GEOPS, 91405, Orsay, France.

[2] Université de Lorraine, CNRS, GeoRessources, 54500 Nancy, France

[3] Caltech, Geological and Planetary Sciences, 91106, Pasadena, CA, USA

[4] Géosciences Rennes, CNRS, Univ Rennes, UMR 6118, F-35000, Rennes, France

[5] Agence Nationale pour La Gestion des Déchets Radioactifs (ANDRA), Centre de Meuse/Haute-Marne, RD 960, 55290 Bure, France

*corresponding author: thomas.blaise@universite-paris-saclay.fr

Keywords

Calcite U-Pb geochronology, Jurassic limestones, Paris Basin, tension gash, far-field deformation

Abstract

Jurassic carbonate strata in the eastern Paris Basin exhibit several generations of faults, tension gashes and stylolites. Although their relative chronology can sometimes be determined according to crosscutting relationships, the duration of major deformation phases and their influence on fluid flow and carbonate cementation are still uncertain. This contribution aims to clarify the timing of brittle deformation and associated calcite cementation. Tension gashes filled by calcite in Jurassic carbonates were sampled in outcrops and boreholes and dated through U-Pb geochronology. Almost all the sampled fractures were cemented during the Cenozoic period. Continuous deformation spreads

from approximately 50 to 30 Ma. Tension gashes oriented N10° to N20° dated at 48 – 43 Ma show the main Pyrenean contractional stage. A second set of calcites were dated around 35-33 Ma and document a Late Eocene - Oligocene extension. A transition from the compressional to the extensional regime is expressed by tension gashes dated between 43 and 35 Ma. Finally, tension gashes oriented N150° to N175°, dated between 32 and 18 Ma, may result from the propagation of the horizontal stress generated by the Alpine orogen or by late Pyrenean deformation. Clumped isotope thermometry on five samples revealed both low crystallization temperatures (from 27 to 53 °C) and also the meteoric origin of calcite-precipitating fluids. Our research therefore documents a continuous fracturing from the Ypresian to the Rupelian, and less expressed brittle deformation during the Miocene period.

1. Introduction

Plate interiors can record far-field deformation as a consequence of tectonic events at their boundaries (e.g., Lacombe et al., 1996; Lacombe & Mouthereau, 1999). The propagation of stress regimes within the intraplate domain may result in long-wavelength folding, reactivation of existing discontinuities, differential erosion of titled blocks and the development of faults, joints, tension gashes or stylolites, especially in sedimentary strata of intracratonic basins (e.g., Bergerat, 1987; Lacombe & Obert, 2000; Parrish et al., 2018). In carbonate rocks, these deformation patterns may enhance fluid flow in permeable strata and favor calcite dissolution-recrystallization, the cementation of primary intergranular porosity or the creation of a secondary pore space (e.g., Bruna et al., 2013). Such far-field deformations have long been recognized in the European plate and paleostress reconstructions were proposed using the inversion of fault slip data or the orientation of calcite twins (e.g., Lacombe et al., 1990).

In the context of radioactive waste storage within sedimentary rocks, the knowledge of the precise chronology of paleostress fields is essential to understand the development of fracture networks and the self-sealing capacities of the sedimentary system (e.g., Sutcliffe et al., 2020). It also brings a source of valuable information regarding the paleo-fluid flow in carbonates and the potential advective flows within claystones

(Mazurek et al., 2018; Pagel et al., 2018). In the eastern Paris Basin, tectonic markers have been investigated in detail within and around the Underground Research Laboratory (URL) of the French National Agency for Radioactive Waste Management (Andra) (André et al. 2010, and references therein). All studies converge in demonstrating that most of the brittle deformations has developed during Cenozoic times. Defining the succession of paleostress regimes from microtectonic analyses in this area is, however, complicated due to many uncertainties. The relation between a tectonic marker and a corresponding deformation event can indeed be ambiguous (e.g., in the eastern Paris Basin, bedding stylolites have developed both during sedimentary burial and in response to extensional stresses during the Eocene – Oligocene, while this portion of the basin was subjected to inversion (André et al., 2010). The cross-cutting relationships and the relative chronology of tectonic features are sometimes unclear (André et al., 2010; Vandeginste et al., 2012; Hoareau et al., 2021). If the same paleostress regime occurred during distinct deformation events, the orientation of tectonic markers may fail to provide genetic information. For instance, in the eastern Paris Basin, NW-SE compression may either be attributed to Late Cimmerian Unconformities (LCU, Guillocheau et al., 2000) during the Jurassic/Cretaceous transition or to Alpine compression during the Miocene (André et al., 2010). Moreover, the orientation of the main stress axes orientation rotated through time during the propagation of contractional deformation related to the Pyrenean and Alpine orogens (André et al., 2010).

Based on the orientation of tension gashes and the petrogeochemical characteristics of calcite filling fractures, vugs, and intergranular pore spaces, Carpentier et al. (2014) proposed a conceptual cementation model for the Middle and Upper Jurassic carbonates in the eastern Paris Basin. The synthetic paragenetic sequence of Carpentier et al. (2014) is based on relative chronologies of cements, fractures, and stylolites, together with the correlation of several petro-geochemical characteristics of calcite cements, including cathodoluminescence, major and trace elemental concentrations, and on oxygen and carbon stable isotope compositions. Such correlations should however be taken with caution, since all these properties are controlled by the physical-chemical parameters prevailing locally during calcite

precipitation, such as the temperature, the intensity of fluid-rock interaction and the fluid/rock ratio, the elemental and isotopic composition of calcite-crystallizing fluids, and finally the vertical and lateral variations in the diagenetic medium (pore sizes, presence of stylolites, composition of the host carbonate rocks).

By contrast, calcite U-Pb geochronology constitutes a far more robust tool to provide absolute temporal correlation of cementation phases and their genetic relationship to large scale brittle deformation events (Hansman et al., 2018; Beaudoin et al., 2018; Lawson et al., 2018; Roberts et al., 2020). So far, three U-Pb ages in calcite cement filling either vugs or fractures were evidenced in the studied area using either isotope dilution-TIMS (Pisapia et al., 2018) or LA-ICP-MS (Pagel et al., 2018; Brigaud et al., 2020). The first age is around 150 Ma, found exclusively in the Middle Jurassic limestones. The second and third ages are around 43 Ma and 33 Ma, respectively. Although these ages offer a better understanding of the cementation events within the studied area, their link with geodynamical events, the duration of deformation (episodic vs. continuous) and the relationship with paleostress regimes remain uncertain. Moreover, the absence of calcite cement younger than ca. 33 Ma puts into question the role of the Alpine orogen located closer to the investigated area when compared to the Pyrenean front. Finally, the origin of fluids involved in calcite precipitation in fractures, vugs, or in the intergranular pore space still requires further investigation. The oxygen stable isotope composition of calcite in tension gashes was systematically measured by André et al., 2010, but the nature of mineralizing fluid was not fully resolved because crystallization temperatures were not known.

In this contribution, we integrated in situ U-Pb geochronology with clumped isotope thermometry in calcite-filled tension gashes, hydraulic breccias and intergranular pore space to constrain the origin, impact and duration of the main deformation phases that affected the eastern Paris Basin. We discuss the nature and temperature of calcite parent fluids and the impact of brittle structures on the cementation of the Middle and Upper Jurassic limestones. We compare our ages obtained on calcite cements with those documented by previous authors in the Paris Basin (Mangenot et al., 2018; Pagel et al., 2018; Pisapia et al., 2018; Brigaud et al., 2020) and in the northern and southern

Pyrenees (Parizot et al., 2021; Cruset et al., 2020, respectively). Our results contribute to the understanding of the relationship between intraplate deformation and the cementation of carbonate rocks in intracratonic sedimentary basins.

2. Geological setting

A detailed view of facies and diagenesis in the Jurassic strata of the eastern Paris Basin is given in Brigaud et al., (2014) and Carpentier et al. (2014). A succession of blocky calcite phases was evidenced, that precipitated either during burial (Vincent et al., 2006; Brigaud et al., 2020), or during the inversion phase that occurred throughout the Cenozoic period (Buschaert et al., 2004; Pagel et al., 2018; Brigaud et al., 2020; Blaise et al., 2022). Blocky calcite of Cenozoic ages precipitated from meteoric fluids (Buschaert et al., 2004) and display a typical dull brown cathodoluminescence (Carpentier et al., 2014). Below, we will first focus on the sedimentary cycles and facies of the Middle and Upper Jurassic limestones, and subsequently on major faults and paleostress regimes.

The Early Bajocian consists of about 30 m-thick bioclastic limestones together with bioherms, called *Calcaires à Polypiers* Formation (Durlet & Thierry, 2000, Brigaud et al., 2014), changing to marly sedimentation during the Early/Late Bajocian transition (*Marnes de Longwy* Formation). A new carbonate ramp then developed in the northeastern Paris Basin from Late Bajocian to Early Callovian, with a typical inner ramp depositional environment (oolitic shoal or lagoon: *Oolites miliaire* and *Calcaires de Chaumont* Formations) at the origin of about 150 m-thick oolithic, bioclastic or mud-dominated limestones (Brigaud et al., 2009). A general flooding of the platform resulting in the deposition of locally thick (>100 m) clay-rich sediments started during the Callovian and lasted until the Early Oxfordian. The carbonate sedimentation started again during the Middle Oxfordian, with about 150 m-thick reefal-dominated limestones (*Complexe récifal* Formation) and oolitic limestones (*Oolithe de Lamothe* and *Oolithe de Saucourt* Formations, Brigaud et al., 2014). Flooding of the platform coeval with a climate cooling (Brigaud et al., 2008; Carpentier et al., 2007; Olivier et al., 2004) favoured a decrease in the carbonate production and the increase of siliciclastic inputs

at the beginning of the Late Oxfordian with the deposition of the *Argiles à huîtres* (Carpentier et al., 2010; Brigaud et al., 2014). A major carbonate production crisis occurred during the Oxfordian/Kimmeridgian transition (Lefort et al., 2011), with marls-dominated sedimentation (*Marnes à Exogyres* Formation), followed by a mixed carbonate, evaporite and siliciclastic ramp environment during the Tithonian (Brigaud et al., 2018).

The major tectonic discontinuities in the eastern Paris Basin are reported in Figure 1. A detailed description of the main fault systems can be found in Le Roux (1980), Bergerat et al. (2007) and André et al. (2010). Some faults correspond to Variscan sutures that later were reactivated during Meso-Cenozoic times, such as the E-W *Vittel* fault, the E-W to NE-SW *Metz* fault and the NNW-SSE to NW-SE *Marne* fault. By contrast, the NNE-SSW *Gondrecourt* and *Joinville* grabens are rooted within the Keuper halite Formation and did not propagate through the basement. These symmetric troughs are related to the European Cenozoic Rift System (ECRIS, Coulon, 1992; Ziegler & Dèzes, 2007; Ring & Gerdes, 2016). Roughly perpendicular to the *Gondrecourt* graben, the *Poissons* fault system constitutes the western border of the area currently investigated by Andra.

At the regional scale, the orientations and relative chronology of minor faults, tension gashes and stylolites can be correlated with the major deformation events recorded in the western European domain during the Meso-Cenozoic period (Bergerat, 1985, 1987; Villemin, 1986; Letouzey, 1986; Coulon & Frizon de Lamotte, 1988; Coulon, 1992; Rocher et al., 2004; Bergerat et al., 2007; André, 2010).

While the Triassic was a period of tectonic quiescence, a first E-W extensional regime is recorded during the Late Triassic and lasts until the Middle Liassic (Guillocheau et al., 2000). A second extension of similar orientation occurred during the Late Jurassic, attributed to the Central Atlantic opening. This regime evolved into an E-W to NE-SW compression during the Early Cretaceous, with two discrete episodes that generated significant uplift and erosion (Guillocheau et al., 2000, Brigaud et al., 2018): (1) The Late Cimmerian Unconformities (LCU) corresponding to a succession of two distinct

truncations in the Paris Basin and (2) the Late Aptian Unconformity (LAU). For some authors however, these Early Cretaceous deformations more likely relate to an extensional regime in the eastern Paris Basin (André et al., 2010).

Early Paleocene NNW–SSE to N–S shortening is reported by André et al. (2010) in the eastern Paris Basin. Briais et al. (2016) show that long wavelength deformation occurred in the central Paris Basin during the intra-Maastrichtian to pre-Thanetian. This deformation, known as the Laramian or Laramide phase (Ziegler et al., 1990), is well documented in western Europe and is coeval with the North Atlantic opening (Briais et al., 2016 and references therein). Briais et al. (2016) document two other deformation phases during the Ypresian: a minor medium-wavelength deformation during Early Ypresian that could be a far-field consequence of the North Atlantic rifting, and a long wavelength deformation during the uppermost Ypresian, with the emersion of the central Paris Basin in response to the convergence between the Iberian and Eurasian plates. So far, these Ypresian phases are not documented in the eastern border of the Paris Basin.

During Eocene times, the Pyrenean compression generated a NNE–SSW transcurrent regime (Pyr1, André et al., 2010) that will rotate into NE-SW (Pyr2, André et al., 2010). According to André et al., (2010), Pyr2 is strongly expressed in the area, but its age remains uncertain. Indeed, for some authors, a NE-SW compression more likely occurred after the Oligocene extension (Bergerat, 1985).

A NW-SE to E-W extension prevailed during the Late Eocene - Oligocene, and the discontinuities generated during the Pyr1 and Pyr2 strike-slip movements were reactivated as normal and oblique faults (Lacombe et al., 1990). The *Gondrecourt* and *Joinville* grabens formed at that time, together with the main grabens constituting ECRIS. Bedding stylolites developed in the Middle and Upper Jurassic carbonates in response to this extensional deformation (Coulon, 1992). Bergerat et al. (2007) considered this Oligocene event as the most strongly expressed in the area.

A ENE–WSW shortening, which post-dates the Oligocene extension was recognized by Bergerat (1987) and André et al. (2010) and may correspond to a later expression of the Pyrenean compression (Pyr3, André et al., 2010).

The Oligocene NW-SE extension switched into a NE-SW extensional regime during the Oligocene - Miocene transition through a σ2/ σ3 permutation. The Alpine compression is then expressed during Miocene-Pliocene times by a clockwise rotation of σ1 from WNW–ESE to NNW–SSE (André et al., 2010).

It is worth noting that, due to the lack of syn-deformation sedimentary record, all age attributions only rely on correlations with the better-constrained tectonic agenda of adjacent domains such as Rhine graben, Alpine belt or Pyrenean domain.

3. Material and methods

3.a. Sampling and petrography

Twenty-seven samples were collected from the Middle Jurassic (Bajocian and Bathonian) and Upper Jurassic (Oxfordian) limestones, from outcrops, quarries, and boreholes (Fig. 1). They mostly correspond to tension gashes filled by calcite affecting mudstones or grainstones from well-identified sedimentary formations (Fig. 2). The orientation of nine tension gashes is reported. Five samples correspond to calcite filling coral or moldic vugs, sometimes connected to fractures. Two samples, collected at Leurville (Fig. 1), are hydraulic breccias found as isolated rock fragments dispersed in agricultural crops. Eleven samples contain several tension gashes, either parallel or crossing each other. In three samples, calcite cements filling the intergranular porosity were targeted for U-Pb geochronology.

Samples were either mounted in epoxy or prepared as 30 µm thin sections and polished. All samples were observed under the optical microscope using transmitted polarized light and under cathodoluminescence (CL) microscopy at 13 keV et 130 mA. For each sample, a series of photomicrographs were gathered to create a composite image (supplementary materials).

3.b. Calcite U-Pb geochronology

The method which has been employed is similar to that described in Brigaud et al. (2020). Sampling and analysis were performed using a Sector Field Inductively Coupled Plasma Mass Spectrometer (SF-ICP-MS) Element XR (Thermo ScientificTM, Waltham, MA, USA) coupled to a 193 nm ArF Laser Ablation System (TELEDYNE, Thousand Oaks, CA, USA) at the Geosciences Paris-Saclay (GEOPS) laboratory of the University of Paris-Saclay.

Samples and calcite reference materials were ablated at a frequency of 8 Hz and a fluence of 1 to 2 $J.cm^{-2}$ with a circular-shaped beam diameter of 150 µm. Glass reference material NIST614 was ablated at a frequency of 10 Hz, a fluence of 6.25 $J.cm^{-2}$ and a beam size of 110 µm. Each analysis consisted of 30 s background acquisition followed by 30 s of sample ablation and 30 s washout. Prior to analysis, each spot was pre-ablated during 4 s at a frequency of 8 Hz and with a fluence of 2 $J.cm^{-2}$. NIST614 was used to correct for $^{207}Pb/^{206}Pb$ fractionation, while $^{238}U/^{206}Pb$ were corrected using WC-1 (Woodhead et al., 2016; Roberts et al., 2017). To ensure accuracy, two secondary calcite reference materials were included in each analytical session: Duff Brown Tank (DBT), dated at 64.0 ± 0.7 Ma by U-Pb isotope dilution (Hill et al., 2016), and B6, dated at 43.0 ± 1.0 Ma by LA-ICP-MS (Pagel et al., 2018). Each analytical sequence is composed of five reference material analyses (one NIST614, one WC-1, one DBT and two B6) inserted at between 10 and 15 spots on unknown calcites. Data was acquired overnight in five sequences of around 400 analyses.

Data was reduced in Iolite© (Paton et al., 2011) using the NIST614 glass as the primary reference material for baseline subtraction, to correct for Pb isotope mass bias and for the estimation of $^{206}Pb/^{238}U$ and $^{207}Pb/^{206}Pb$ instrumental drift over the sequencing time. No down-hole fractionation correction is applied in Iolite© (Nuriel et al., 2017).

The 2 standard errors in the mean $^{207}Pb/^{206}Pb$ and $^{206}Pb/^{238}U$ ratios measured on NIST614 during the analytical session were propagated to the final age uncertainty of all calcite samples by quadratic addition. Data was plotted on Tera-Wasserburg graphs using IsoplotR online (Vermeesch, 2018), without anchoring the initial $^{207}Pb/^{206}Pb$ value. Error ellipses of each spot and the error in the Tera-Wasserburg intercept age are at a level of two sigma. In each Tera-Wasserburg graph, a first age uncertainty is given that

does not include uncertainty propagations. A second age uncertainty is given, by propagating the systematic uncertainty of the age of primary reference material WC-1 (2.6%), and the 2 standard errors of the $^{207}Pb/^{206}Pb$ and $^{206}Pb/^{238}U$ of the analytical session by quadratic addition. Sample ages and uncertainties are listed in Table 1 and detailed metadata for LA-ICP-MS calcite U-Pb geochronology is available in supplementary materials.

3.d. Oxygen and carbon stable isotope composition and clumped isotope thermometry

For oxygen and carbon stable isotope analysis, eleven calcite crystals from fracture in-fills were fragmented and collected with tweezers under the magnifying glass. The crystals were subsequently grounded into a homogeneous powder in an agate mortar. Oxygen and carbon isotopes were analysed in the Geosciences Laboratory of Rennes University (France) following the methodology described in Malfilatre, 2012. All isotopic values are reported to the V-PDB standard (Table 2).

Five samples consisting of large in-fillings were selected for clumped isotope analysis. 30 mg of calcite was sampled using a micro-drilling tool. Δ_{47} measurements were performed at the California Institute of Technology (USA) in two analytical sessions (April and May 2021) with an automated acid digestion and gas purification device coupled to a dual inlet Thermo MAT253, as described in Passey et al., 2010. Samples were weighed into silver capsules (~ 8 mg) and reacted in a common phosphoric acid bath (~ 103 %) for 20 minutes at 90 °C under static vacuum. The resulting CO_2 was passed through an ethanol/dry ice U-trap (~ –80 °C) before being collected on a liquid nitrogen temperature (–196 °C) U-trap. Following the 20 minutes reaction period, the collected CO_2 was thawed, entrained in helium, and carried through a Porapak Q 120/80 mesh gas column held at –20 °C using He as the carrier gas. The purified CO_2 was analyzed using a Thermo Scientific MAT 253 Mass Spectrometer set to collect masses 44-49. Mass 48 was only monitored to detect any hydrocarbon contaminant. $\delta^{18}O$ and $\delta^{13}C$ data was also acquired as part of each Δ_{47} analysis and calculated using the parameters reported relative to the PDB reference frame based on the calibrated composition of the laboratory working gas and the correction scheme and constants from Brand et al., (2010). In order to account for the temperature dependence of oxygen

isotope fractionation between CO_2 gas and carbonate resulting from the reaction with phosphoric acid at 90 °C, a fractionation factor of 1.00811 was used for calcite (following Swart et al., 1991). The raw Δ_{47} data was corrected for instrument non-linearity and scale compression (Dennis et al., 2011) using several heated (at 1000°) and equilibrated gases (at 25°C) of various bulk isotopic compositions that were run during each session. These gases were used to convert measurements into the inter-laboratory absolute reference frame (Dennis et al., 2011). To guarantee accuracy of the Δ_{47} data, we routinely analyzed two carbonate reference materials (Carrara marble and TV04). One of these two carbonate standards was analyzed once for every five analyses of the unknown samples in order to check for procedural analytical stability and accuracy, and to determine the long-term external reproducibility of our measurements. The Δ_{47} values obtained for these carbonates over the course of this study (May to July 2019) are: $\Delta_{47\text{-CDES25}}$ = 0.409 ± 0.016‰ (1SD, n = 10) for Carrara; $\Delta_{47\text{-CDES25}}$ = 0.666 ± 0.011‰ (1SD, n = 8) for TV04, i.e., within accepted Δ_{47} values for TV04 ($\Delta_{47\text{-CDES25}}$ = 0.655‰) and Carrara ($\Delta_{47\text{-CDES25}}$ = 0.405‰). Finally, the corrected Δ_{47} values were converted into temperatures using the composite Δ_{47}-T calibration of Bonifacie et al. (2017), which has been shown to be appropriate for calcite and dolomite between 0 and 300 °C, and which has been shown to be consistent with measurements made at Caltech. The oxygen isotopic compositions of the water ($\delta^{18}O_{water}$) from which the carbonates precipitated were calculated for each estimated $T\Delta_{47}$ using the bulk $\delta^{18}O_{carb}$ values and the calcite-water fractionation equation from O'Neil et al. (1969).

4. Results

4.a. Calcite petrography

All samples consist of blocky calcite filling tension gashes (Fig. 3) and vugs, apart from the hydraulic breccia sampled at Leurville (LEU samples, Fig. 4). Crystal sizes vary from a few hundred micrometers in small tension gashes to a few millimeters in hydraulic breccias. No syntaxial or antitaxial growth orientation are identified (*sensu* Bons et al., 2012). While most samples contain clean crystals, a few of them (e.g., SOM1-1, SOM1-2, REM1) incorporated micrite inclusions from the host rocks during crystallisation (Fig. 5). Most samples contain non-luminescent or weakly brown luminescent crystals under

CL, without clear successive growth stages. No evidence of multi-phase fracture opening was observed. Apart from samples SOR6-c and DGSM29-1, all fractures are entirely cemented by blocky calcite. No dissolution features, such as corrosion gulfs, were observed. Samples SR6 and SOR6 display ambiguous cross-cutting relationships between at least two distinct generations of tension gashes that are filled with calcite displaying the same cathodoluminescence (Fig. 6). Petrographic illustrations of all samples are available in supplementary materials.

4.b. U-Pb ages

Among the 27 samples collected for the purpose of this study, 4 were not amenable to U-Pb geochronology and were thus excluded. A total of 32 U-Pb ages are reported (Table 1). The oldest age measured in tension gashes is found in the Upper Bathonian sampled in the Montcornet borehole (sample A901-22), dated at 92.9 ± 10.3 Ma. In the same sample, another population of tension gashes is dated at 68.4 ± 4.0 Ma. In the Sarazinère quarry, a tension gash oriented N50 (sample SR6a) gives an age of 58.9 ± 1.8 Ma. Most of the ages obtained are between 50.4 ± 2.4 Ma (sample PPA1073) and 27.4 ± 2.8 Ma (sample MXV9a). A hydraulic breccia sampled at Leurville (sample LEU-2) gives an age of 22.2 ± 1.2 Ma. Finally, a tension gash oriented N150 gives a younger age of 18.7 ± 1.0 Ma (sample SR6b).

In addition, three ages were measured in the intergranular calcite cements, yielding ages of 100.9 ± 22.7 Ma (sample A901-22e), 57.7 ± 2.6 Ma (sample SR6c), and 30.6 ± 7.0 Ma (sample DGSM29-2b).

4.c. Oxygen and carbon stable isotope composition and clumped isotopes

$\delta^{18}O$ values range between –7.0 ‰$_{V\text{-}PDB}$ (sample SOR6ab) and –10.5 ‰$_{V\text{-}PDB}$ (samples BAZX90a and LEU1-1), while $\delta^{13}C$ are between 1.1 ‰$_{V\text{-}PDB}$ (sample A901-22a) and 3.4 ‰$_{V\text{-}PDB}$ (sample VCLD). $\delta^{18}O$ and $\delta^{13}C$ values measured by clumped isotopy are identical within the limits of analytical uncertainty to the ones obtained from the traditional method where C and O stable isotope compositions are measured separately. The highest Δ_{47} temperature is obtained for sample BAZX90a (53 ± 5 °C), and the lowest for sample SR6b (27 ± 3 °C). Three other samples give temperatures of

37 ± 2 °C (VCLD), 41 ± 1 °C (25209) and 42 ± 2 °C (25229). Sample types and associated isotopic values are summarized in Table 2.

5. Discussion

5.a Ages, impact and duration of brittle deformation

Since no syntaxial or antitaxial growth orientation were identified (sensu Bons et al., 2012), the syn-kinematic precipitation of calcite crystals within tension gashes is unclear (Roberts and Holdsworth (2022). Field observations have revealed that tension gashes are generally associated with tectonic stylolites, suggesting syn-kinematic calcite dissolution and recrystallization (André et al., 2010). Furthermore, although CL sectorial zoning is observed in some samples, no successive calcite growth stages can be clearly determined, suggesting that all crystals filling a given tension gash or vug are monogenic. An isochron obtained from the sampling of several crystals filling a given tension gash proves that calcite formed during a single precipitation event. Yet, calcite cements can post-date fracture opening. Such uncertainty is somehow minimized by the large number of samples considered for this research, and by the good agreement between the orientation of fractures and their U-Pb ages, which will be discussed below.

Calcite mechanical twinning is observed in some samples (LEU1-1, VCLD, BAZX90a, REM-3-2, REM1, OT-1-2, SOM1-1, SOM1-2). The development of such twinning cannot be correlated with the age or location of the samples. The absence of calcite twinning in most samples may be due to the small size of blocky calcite crystals filling tension gashes (Lacombe et al., 1990).

The tension gash showing the oldest age was sampled in the Montcornet borehole, located around 200 km north-west of the Andra URL, in the vicinity of the Ardennes massif (Fig. 1). The U-Pb age of 92.9 ± 10.3 Ma suggests the Albian to Santonian period that may be related to a major inversion phase documented in northern France (Bergerat & Vandycke, 1994). Interestingly, this calcite U-Pb age matches with the age obtained on the first dolomite cement identified in the Middle Jurassic at depth in the central Paris Basin (Mangenot et al., 2018). Our data agrees with André et al. (2010) and tends to indicate the absence of this tectonic phase around the Andra URL. Another

sample in the same borehole was dated at 68.4 ± 4.0 Ma, i.e., the Cretaceous-Paleocene transition (Fig. 7). This age cannot be confidently interpreted and attributed to a known deformation phase. It may either be linked to the so-called “sub-hercynian” inversion phase defined by Ziegler (1987) or to an early stage of the Pyrenean compression, as evidenced in the south-eastern Pyrenees (Cruset et al., 2020). In the central Paris Basin, a second blocky calcite generation was also dated at 68.5 ± 7.7 Ma in the deep Middle Jurassic (Mangenot et al., 2018). Whatsoever, these early phases recorded here more than 150 km north or west of the URL are not described in the eastern Paris Basin, where brittle structures are mostly thought to be Cenozoic in age (André et al., 2010; Bergerat et al., 2007, this study). Indeed, the ages of tension gashes and hydraulic breccias documented here span from 58.9 ± 1.8 Ma to 18.7 ± 1.0 Ma, i.e., from the Thanetian to the Burdigalian periods (Fig. 7).

Our data show that tectonic quiescence then prevailed during the Paleocene and Early Ypresian, a result in agreement with the slow rate of N-S convergence between the Iberian and Eurasian plates during this period (Mouthereau et al., 2021; Grool et al., 2018; Macchiavelli et al., 2017). A single tension gash oriented N50° is dated at 58.9 ± 1.8 Ma (Paleocene) in the Sarazinière quarry. This fracture may be related to an early stage of the Pyrenean compression. Alternatively, this event may be linked to the so-called “Laramide” phase (Ziegler, 1987), which corresponds to a major inversion period with an uplift and erosion quantified to about 600 m in the Morvan Massif, south of the Paris Basin, and to 300 m in the study area (Barbarand et al., 2013, Blaise et al., 2014). This event does not seem to be restricted to the eastern border of the Paris Basin, since a U-Pb age of 61.1 ± 2.5 was documented for calcite cements in the Middle Jurassic at depth in the central Paris Basin (Mangenot et al., 2018).

A continuous deformation is then recorded in the age distribution of tension gashes from the Late Ypresian to the Rupelian, although two age clusters can be evidenced between 40-50 Ma (9 samples) and 30-35 Ma (7 samples) (Fig. 7). The first age cluster (40-50 Ma) is associated to N10° to N20° tension gashes (BAZX90a, MXV7, VCLD). The Late Ypresian to Bartonian opening and filling of these gashes probably record the far-field onset of the main Pyrenean compressional event at that time (Macchiavelli et al., 2017).

Within this deformation phase, discrete tectonic pulses may have generated higher rates of fracturing. A cluster of ages is recorded at ca. 48 Ma (samples A00607c, SOR6ab, SOR6c, BAZX90a), synchronous to the emersion of the central Paris Basin (Briais et al., 2016) in response to the main Pyrenean compression period (e.g., Cruset et al., 2020). Several tension gashes are then dated at ca. 43 Ma (Fig. 7), matching the U-Pb ages reported by Pagel et al. (2018) along the Gondrecourt graben and the age of a vertical tension gash in HTM102 borehole close to the Andra URL (Brigaud et al., 2020).

A reactivation of the variscan Vittel fault south of the studied area is evidenced by two fractures sampled in the Sommerécourt quarry and dated at 42.5 ± 3.9 Ma and 40.9 ± 1.7 Ma (Fig. 7). At Removille, sample REM1 was collected along a fault delimiting a small graben of similar orientation to the Gondrecourt and Joinville grabens. The age of this sample, 42.1 ± 2.7 Ma confirms the synchronous formation of these structures. Finally, sample OT1-2 from the Ottange quarry dated at 40.8 ± 2.2 Ma demonstrates that this intraplate deformation extended far north of the study area (Fig. 1). They are also recorded in the central Paris Basin, as documented by Mangenot et al. (2018). These deformations and cementations are all interpretated as a far-field consequence of Pyrenean shortening.

A few fractures are dated between 40 and 35 Ma, while another main fracturing event is identified at around 33 Ma (Fig. 7, Table 1). Ten of the 32 measured U-Pb ages obtained are in the 35-30 Ma range, matching previous U-Pb ages around 33 Ma reported for fractures along the Gondrecourt faults (Pagel et al., 2018) and vug-filling calcites in Oxfordian limestones from the Andra URL borehole cores (Pisapia et al., 2018). Following Pagel et al. (2018) by analogy with the known tectonic agenda of the Rhine Graben, we suggest that these dated structures are related to extensional deformation and the opening of the ECRIS (Dezès et al., 2004; Bergerat et al., 2007; Ring & Gerdes, 2016), an event that is strongly expressed in the eastern Paris Basin (Bergerat et al., 2007) as attested by the formation of the small Gondrecourt and Joinville grabens. A second generation of tension gashes collected along the Removille graben (REM3-2) yield an age of 31.7 ± 3.8 Ma, showing that this graben was formed

through a two-step evolution identical to the Gondrecourt graben, i.e., a strike-slip or oblique displacement during the Lutetian, followed by extension during the Rupelian.

On the other hand, we cannot fully exclude a compressional origin for all of these ca. 33 Ma tension gashes as a consequence of further Pyrenean or Alpine far-field deformations (Cruset et al., 2020; Parizot et al., 2021). Whatsoever, we show here that deformation in the eastern Paris Basin occurred continuously from the Late Ypresian to the Rupelian (Fig. 7) and that the transition from a contractional regime prevailing during the Eocene period to an extensional deformation during the Oligocene may have been progressive.

After this 33 Ma ECRIS-related event, few younger gashes are dated around 30 Ma. Tension gashes developed in the quarries of Dugny-sur-Meuse and Maxey-sur-Vaise dated around 32-27 Ma are oriented N170° and N175° and may have opened during a compressional phase documented by Bergerat (1987) and André et al. (2010) and interpreted as a late Pyrenean horizontal stress. This age also replicates the ones obtained by Parizot et al. (2021) in the north Pyrenean foreland basin, and those of Cruset et al. (2020) in the southern Pyrenees, interpreted as a short-living reactivation of the compression at that time and whose expression is recorded up to the southern coast of England (Parrish et al., 2018). Alternatively, such tension gashes could have formed in response to a NE-SW extension generated from an interchange between σ2 and σ3 (André et al., 2010).

Post-Rupelian brittle structures are scarce (Fig. 7). The absence of tension gashes dated between around 27 Ma and 22 Ma suggests a period of quiescence during Chattian before the renewal of compressive deformation. Calcite-cemented hydraulic breccias affecting the Oolithe de Saucourt Formation precipitated during the Chattian – Aquitanian period. In the Sarazinière quarry, a tension gash oriented N150° gave a younger age of 18.7 ± 1.0 Ma. Thus, this renewal of deformation had a limited impact on the opening of fractures in the eastern Paris Basin. This is in agreement with field observations that documented poorly-developed tectonic microstructures related to Miocene times (André et al., 2010), and the absence of reactivation of the main discontinuities (Bergerat et al., 2007).

Both Miocene calcites were sampled in the vicinity of the NW-SE Poissons fault system (Fig. 1) that reactivated in response to the compression during either the earliest stages of the Alpine contractional stress or a Late Pyrenean event during Aquitanian/Burdigalian (Parizot et al., 2021 ; Hoareau et al., 2021).

Finally, the absence of younger ages indicates that the growth of the nearby Jura fold-and-thrust belt formed roughly between 11 and 3 Ma (Homberg et al., 2002; Smeraglia et al., 2021) had no or very limited impact on the deformation of the eastern Paris Basin.

To sum up, the deformation of the eastern Paris Basin is essentially related to far-field propagation of compressional stress during the Pyrenean orogen growth. It has been accommodated continuously by the opening of tension gashes and the development or reactivation of strike-slip faults and stylolites between around 50 Ma (sample PPA1073) and 27 Ma (sample MXV9a), with deformation pulses at ca. 48 Ma and 43 Ma, and only interrupted shortly by the ECRIS-related extensional event at around 33 Ma.

On a larger scale, this tectonic agenda of the eastern Paris Basin is consistent with the U-Pb ages of slickenfibres and fracture filling calcites in the north foreland basin of the Pyrenees (Parizot et al., 2021), in the southeastern Pyrenean fold and thrust belt and the south foreland Ebro basin (Cruset et al., 2020) and along the Cevennes fault system (Parizot et al., 2022). South of the Paris Basin, fluorite mineralization occurred likely in response of this contractional event (Lenoir et al., 2021). This event is also recorded in the Jura fold-and-thrust belt, where a pre-orogenic NE-SW strike-slip fault was recently evidenced through U-Pb geochronology of slickenfibre calcite yielding two ages similar to ours at 48.4 ± 1.5 and 44.7 ± 2.6 Ma (Smeraglia et al., 2021).

5.b. Origin and Temperature of calcite-mineralizing fluids

The meteoric origin of waters from which calcite precipitated in tension gashes was suggested by André et al. (2010) on the basis of the $\delta^{18}O$ values measured in calcite. Yet, the oxygen stable isotope composition of parent-waters was uncertain, since the fractionation factor between H_2O and calcite was estimated from only six two-phased aqueous fluid inclusions that homogenized at temperatures ranging from 31 to 38 °C (Buschaert et al., 2004). Thanks to the Δ_{47} clumped isotope composition of calcite, the

origin of parent-waters can be determined with a higher level of confidence, especially in low-temperature environments in which aqueous inclusions remain in a single-phase metastable state (Goldstein & Reynolds, 1994). The $\delta^{18}O$ values of calcite-mineralizing waters determined on five samples from their clumped isotope composition, range from –4.6 to –2.6 $‰_{V\text{-}SMOW}$, supporting the views of André et al. (2010) and Pagel et al. (2018) regarding its meteoric origin.

The temperature at which calcite cements precipitated in veins and hydraulic breccias along the Gondrecourt graben was lower than 50 °C (Pagel et al., 2018), slightly higher than the expected temperature of the host rock. Yet, Brigaud et al. (2020) reported higher temperatures, up to 90 °C, in a calcite-filled tension gash dated at 41.5 ± 4.8 Ma at the vicinity of the Gondrecourt graben (well HTM102 located 2 km from the graben, Fig. 7). These temperatures suggest that hot fluid flow migrated along deeply rooted faults during the Ypresian/Bartonian compressional regime (Brigaud et al., 2020). Here, the highest Δ_{47} temperature is around 53 °C in the *Calcaires de Chaumont* Formation (Bathonian), showing that meteoric waters were slightly in thermal disequilibrium with their host rocks. In such case, meteoric waters from deeper strata may have risen upward through the fracture network (Ge & Garven, 1992; Sibson, 1994). In addition, the Δ_{47} temperatures may also reflect the burial depth at which calcite precipitation occurred: the oldest fractures may have developed at a depth of 700 to 1000 m. Since the eastern Paris Basin experienced inversion and associated erosion during Cenozoic times, the youngest fractures (Miocene) were generated closer to the present-day surface (Fig. 8).

5.c. Origin of intergranular calcite cements

The impact of Cenozoic intraplate deformation in the interparticle cementation of the Jurassic limestones in the eastern Paris Basin is still unclear. André et al. (2010) and Carpentier et al. (2014) stressed that contractional deformation generated vertical stylolites with horizontal peaks and that a high density of bed-parallel stylolites could be attributed to the Late Eocene – Oligocene extensional period. These tectonic stylolites developed during the inversion of the eastern Paris Basin and may have contributed to calcite dissolution-recrystallization and eventually to the cementation of intergranular

pores (Buschaert et al., 2003; André et al., 2010). This scenario is supported by recent U-Pb ages of vug-filling calcite in the Oxfordian limestones at ca. 33 Ma (Pisapia et al., 2018), showing that the Late Eocene – Oligocene extension effectively contributed to occlude the pore space.

Among the samples considered for this research, three display blocky calcite cementing the intergranular porosity large enough to be targeted for U-Pb dating. In sample DGSM29-2, these blocky calcites yielded an age of 30.6 ± 7.0 Ma (DGSM29-2b, table 1), identical, within the limits of analytical uncertainties, to the age of the nearby N170 tension gashes (DGSM29-2a and DGSM29-1) at 32.0 ± 1.5 Ma and 31.6 ± 2.9 Ma. In sample A901-22, blocky calcite cements filling intergranular pores are dated at 100.9 ± 22.7 Ma (A901-22e), matching the age of the nearby fracture dated at 92.9 ± 10.3 Ma (A901-22a). However, age uncertainties are large for this sample, which may be explained by low U/Pb ratios together with the presence of a younger calcite infilling fractures (A901-22c, dated at 68.4 ± 4 Ma), which may have induced the dissolution-recrystallization of the older calcite cement. A third example is illustrated in figure 9 with a grainstone sampled at the Sarazinière quarry (*oolithe de Lamothe* Formation, Upper Oxfordian), affected by two generations of tension gashes. The first generation is oriented N50° and yields an age of 58.9 ± 1.8 Ma (SR6a), while the second is oriented N150° and is dated at 18.7 ± 1.1 Ma (SR6b). Both tension gashes are filled by calcite crystals displaying the same cathodoluminescence (Fig. 9), hence the difficulty to establish a relative chronology from their cross-cutting relationship. Calcite U-Pb geochronology resolves this issue. Moreover, the intergranular pore space is entirely plugged by a blocky calcite showing a comparable dull brown cathodoluminescence. The U-Pb age of this blocky calcite, 57.7 ± 2.6 Ma (SR6c) is identical to the older tension gash (SR6a, 58.9 ± 1.8 Ma). It is worth noting that these ages match the one obtained on the second blocky calcite generation in the deep Middle Jurassic carbonate strata from the Paris Basin depocenter (Mangenot et al. 2018).

Therefore, although tension gashes could have acted as preferential conduits for meteoric waters, fluid flow and associated calcite crystallization were not only restricted to the fracture network. Paleo-water flows through the intergranular porosity and

subsequent cementation was enhanced by the development of brittle microstructures (Hansman et al., 2018; Sun et al., 2022). This is shown by the synchronous precipitation of calcite in tension gashes and in the adjacent intergranular pore space. However, the spatial extension of such “tectonic-induced cementation” is unknown and needs further research and complementary geochronological data on calcite cements occluding the intergranular pore space.

6. Conclusions

We have provided evidence for a continuous fracturing of the Jurassic carbonates from the Ypresian to the Rupelian in the eastern Paris Basin. This period coincides with the main shortening related to the Pyrenean orogen growth, interrupted by extensional deformation during Late Eocene – Early Oligocene. Three U-Pb age clusters are identified, the two firsts at around 48 Ma and 43 Ma, related to the far-field propagation of Pyrenean horizontal stress, and a third at 33 Ma corresponding to the ECRIS-related extensional regime. Fluids of meteoric origin percolated through the fracture networks at rather low temperatures (from 27 to 53 °C), with a progressive decrease of temperature though time. Fluid flow and associated calcite precipitation was not restricted within the fractures, but also occurred in the intergranular pore space.

Acknowledgements

This manuscript benefited from fruitful discussion with Christian Hibsch. We also thank Frédéric Haurine for his assistance during the LA-ICP-MS U-Pb analysis. This work is the outcome of collaborative project between the University Paris-Saclay and Andra, the French agency for radioactive waste management, funded in part by Andra. We thank the two anonymous reviewers for their constructive comments that helped to improve the manuscript.

Declaration of interest

The authors declare none

References

ANDRE, G., HIBSCH, C., FOURCADE, S., CATHELINEAU, M. & BUSCHAERT, S. 2010. Chronology of fracture sealing under a meteoric fluid environment: Microtectonic and isotopic evidence of major Cainozoic events in the eastern Paris Basin (France). *Tectonophysics* **490**, 214–228.

BARBARAND, J., QUESNEL, F. & PAGEL, M. 2013. Lower Paleogene denudation of Upper Cretaceous cover of the Morvan Massif and southeastern Paris Basin (France) revealed by AFT thermochronology and constrained by stratigraphy and paleosurfaces. *Tectonophysics* **608**, 1310–1327.

BEAUDOIN, N., LACOMBE, O., ROBERTS, N.M.W. & KOEHN, D. 2018. U-Pb dating of calcite veins reveals complex stress evolution and thrust sequence in the Bighorn Basin, Wyoming, USA. *Geology* **46**, 1015–1018.

BERGERAT, F. 1985. Déformations cassantes et champs de contrainte tertiaires dans la plate-forme européenne. PhD thesis, Université Pierre et Marie Curie - Paris VI, 365. Published thesis.

BERGERAT, F. 1987. Stress fields in the European platform at the time of Africa-Eurasia collision. *Tectonics* **6**, 99–132.

BERGERAT, F. & VANDYCKE, S. 1994. Palaeostress analysis and geodynamical implications of Cretaceous-Tertiary faulting in Kent and the Boulonnais. *Journal of the Geological Society* **151**, 439–448.

BERGERAT, F., ELION, P., FRIZON DE LAMOTTE, D., PROUDHON, B., COMBES, P., ANDRÉ, G., WILLEVEAU, Y., LAURENT-CHARVET, S., KOURDIAN, R., LEROUGE, G. & OTT D'ESTEVOU, P. 2007. 3D multiscale structural analysis of the Eastern Paris Basin : the ANDRA contribution. *Mémoire de la Société Géologique de France* **178**, 15–35.

BLAISE, T., BARBARAND, J., KARS, M., PLOQUIN, F., AUBOURG, C., BRIGAUD, B., CATHELINEAU, M., EL ALBANI, A., GAUTHERON, C., IZART, A., JANOTS, D., MICHELS, R., PAGEL, M., POZZI, J.-P., BOIRON, M.-C. & LANDREIN, P. 2014. Reconstruction of

low temperature (<100 °C) burial in sedimentary basins: A comparison of geothermometer in the intracontinental Paris Basin. *Marine and Petroleum Geology* **53**, 71–87.

BLAISE, T., CATHELINEAU, M., BOULVAIS, P., TECHER, I., BOIRON, M.-C., TARANTOLA, A., BRIGAUD, B. & LANDREIN, P. 2022. Origin of 87Sr enrichment in calcite cements in Jurassic limestones (Eastern Paris Basin, France). *Applied Geochemistry* **136**, 105–131.BONIFACIE, M., CALMELS, D., EILER, J.M., HORITA, J., CHADUTEAU, C., VASCONCELOS, C., AGRINIER, P., KATZ, A., PASSEY, B.H., FERRY, J.M. & BOURRAND, J.-J. 2017. Calibration of the dolomite clumped isotope thermometer from 25 to 350 °C, and implications for a universal calibration for all (Ca, Mg, Fe)CO3 carbonates. *Geochimica et Cosmochimica Acta* **200**, 255–279.

BONS, P.D., ELBURG, M.A. & GOMEZ-RIVAS, E. 2012. A review of the formation of tectonic veins and their microstructures. *Journal of Structural Geology* **43**, 33–62.

BRAND, W.A., ASSONOV, S.S. & COPLEN, T.B. 2010. Correction for the ^{17}O interference in $\delta(^{13}C)$ measurements when analyzing CO_2 with stable isotope mass spectrometry (IUPAC Technical Report). *Pure and Applied Chemistry* **82**, 1719–1733.

BRIAIS, J., GUILLOCHEAU, F., LASSEUR, E., ROBIN, C., CHÂTEAUNEUF, J.J. & SERRANO, O. 2016. Response of a low-subsiding intracratonic basin to long wavelength deformations: the Palaeocene–early Eocene period in the Paris Basin. *Solid Earth* **7**, 205–228.

BRIGAUD, B., PUCÉAT, E., PELLENARD, P., VINCENT, B. & JOACHIMSKI, M.M. 2008. Climatic fluctuations and seasonality during the Late Jurassic (Oxfordian–Early Kimmeridgian) inferred from $\delta^{18}O$ of Paris Basin oyster shells. *Earth and Planetary Science Letters* **273**, 58–67.

BRIGAUD, B., DURLET, C., DECONINCK, J.-F., VINCENT, B., PUCÉAT, E., THIERRY, J. & TROUILLER, A. 2009. Facies and climate/environmental changes recorded on a carbonate ramp: A sedimentological and geochemical approach on Middle

Jurassic carbonates (Paris Basin, France). *Sedimentary Geology* **222**, 181–206.

BRIGAUD, B., VINCENT, B., CARPENTIER, C., ROBIN, C., GUILLOCHEAU, F., YVEN, B. & HURET, E. 2014. Growth and demise of the Jurassic carbonate platform in the intracratonic Paris Basin (France): Interplay of climate change, eustasy and tectonics. *Marine and Petroleum Geology* **53**, 3–29.

BRIGAUD, B., VINCENT, B., PAGEL, M., GRAS, A., NORET, A., LANDREIN, P. & HURET, E. 2018. Sedimentary architecture, depositional facies and diagenetic response to intracratonic deformation and climate change inferred from outcrops for a pivotal period (Jurassic/Cretaceous boundary, Paris Basin, France). *Sedimentary Geology* **373**, 48–76.

BRIGAUD, B., BONIFACIE, M., PAGEL, M., BLAISE, T., CALMELS, D., HAURINE, F. & LANDREIN, P. 2020. Past hot fluid flows in limestones detected by Δ_{47}–(U-Pb) and not recorded by other geothermometers. *Geology* **48**(9), 851–856.

BRUNA, P.-O., GUGLIELMI, Y., LAMARCHE, J., FLOQUET, M., FOURNIER, F., SIZUN, J.-P., GALLOIS, A., MARIÉ, L., BERTRAND, C. & HOLLENDER, F. 2013. Porosity gain and loss in unconventional reservoirs: Example of rock typing in Lower Cretaceous hemipelagic limestones, SE France (Provence). *Marine and Petroleum Geology* **48**, 186–205.

BUSCHAERT, S., FOURCADE, S., CATHELINEAU, M., DELOULE, E., MARTINEAU, F., AYT OUGOUGDAL, M. & TROUILLER, A. 2004. Widespread cementation induced by inflow of continental water in the eastern part of the Paris basin: O and C isotopic study of carbonate cements. *Applied Geochemistry* **19**, 1201–1215.

CARPENTIER, C., LATHUILIÈRE, B., FERRY, S. & SAUSSE, J. 2007. Sequence stratigraphy and tectonosedimentary history of the Upper Jurassic of the Eastern Paris Basin (Lower and Middle Oxfordian, Northeastern France). *Sedimentary Geology* **197**, 235–266.

CARPENTIER, C., LATHUILIÈRE, B. & FERRY, S. 2010. Sequential and climatic framework of

the growth and demise of a carbonate platform: implications for the peritidal cycles (Late Jurassic, North-eastern France): Growth and demise of a carbonate platform. *Sedimentology* **57**, 985–1020.

CARPENTIER, C., BRIGAUD, B., BLAISE, T., VINCENT, B., DURLET, C., BOULVAIS, P., PAGEL, M., HIBSCH, C., YVEN, B., LACH, P., CATHELINEAU, M., BOIRON, M.-C., LANDREIN, P. & BUSCHAERT, S. 2014. Impact of basin burial and exhumation on Jurassic carbonates diagenesis on both sides of a thick clay barrier (Paris Basin, NE France). *Marine and Petroleum Geology* **53**, 44–70.

COULON, M. 1992. La Distension oligocene dans le nord-est du bassin de Paris (perturbation des directions d'extension et distribution des stylolites). *Bulletin de la Société Géologique de France* **163**, 531–540.

COULON, M. & FRIZON DE LAMOTTE, D. 1988. Les craies eclatees du secteur d'Omey (Marne, France); le resultat d'une brechification par fracturation hydraulique en contexte extensif. *Bulletin de la Société Géologique de France* **4**, 177–185.

CRUSET, D., VERGÉS, J., ALBERT, R., GERDES, A., BENEDICTO, A., CANTARERO, I. & TRAVÉ, A. 2020. Quantifying deformation processes in the SE Pyrenees using U–Pb dating of fracture-filling calcites. *Journal of the Geological Society* **177**, 1186–1196.

DENNIS, K.J., AFFEK, H.P., PASSEY, B.H., SCHRAG, D.P. & EILER, J.M. 2011. Defining an absolute reference frame for 'clumped' isotope studies of CO_2. *Geochimica et Cosmochimica Acta* **75**, 7117–7131.

DURLET, C. & THIERRY, J. 2000. Modalites sequentielles de la transgression aaleno-bajocienne sur le sud-est du Bassin parisien. *Bulletin de la Société Géologique de France* **171**, 327–339.

GE, S. & GARVEN, G. 1992. Hydromechanical modeling of tectonically driven groundwater flow with application to the Arkoma Foreland Basin. *Journal of Geophysical Research* **97**, 9119–9144.

GOLDSTEIN, R.H. & REYNOLDS, T.J. 1994. *Systematics of Fluid Inclusions in Diagenetic Minerals*, SEPM Society for Sedimentary Geology

GROOL, A.R., FORD, M., VERGÉS, J., HUISMANS, R.S., CHRISTOPHOUL, F. & DIELFORDER, A. 2018. Insights Into the Crustal-Scale Dynamics of a Doubly Vergent Orogen From a Quantitative Analysis of Its Forelands: A Case Study of the Eastern Pyrenees. *Tectonics* **37**, 450–476.

GUILLOCHEAU, F., ROBIN, C., ALLEMAND, P., BOURQUIN, S., BRAULT, N., DROMART, G., FRIEDENBERG, R., GARCIA, J.-P., GAULIER, J.-M., GAUMET, F., GROSDOY, B., HANOT, F., LE STRAT, P., METTRAUX, M., NALPAS, T., PRIJAC, C., RIGOLTET, C., SERRANO, O. & GRANDJEAN, G. 2000. Meso-Cenozoic geodynamic evolution of the Paris Basin: 3D stratigraphic constraints. *Geodinamica Acta* **13**, 189–245.

HANSMAN, R.J., ALBERT, R., GERDES, A. & RING, U. 2018. Absolute ages of multiple generations of brittle structures by U-Pb dating of calcite. *Geology* **46**, 207–210.

HILL, C.A., POLYAK, V.J., ASMEROM, Y. & P. PROVENCIO, P. 2016. Constraints on a Late Cretaceous uplift, denudation, and incision of the Grand Canyon region, southwestern Colorado Plateau, USA, from U-Pb dating of lacustrine limestone. *Tectonics* **35**, 896–906.

HOAREAU, G., CROGNIER, N., LACROIX, B., AUBOURG, C., ROBERTS, N.M.W., NIEMI, N., BRANELLEC, M., BEAUDOIN, N. & SUÁREZ RUIZ, I. 2021. Combination of Δ_{47} and U-Pb dating in tectonic calcite veins unravel the last pulses related to the Pyrenean Shortening (Spain). *Earth and Planetary Science Letters* **553**, 116636.

HOMBERG, C., BERGERAT, F., PHILIPPE, Y., LACOMBE, O. & ANGELIER, J. 2002. Structural inheritance and cenozoic stress fields in the Jura fold-and-thrust belt (France). *Tectonophysics* **357**, 137–158.

KIM, S.-T., COPLEN, T.B. & HORITA, J. 2015. Normalization of stable isotope data for carbonate minerals: Implementation of IUPAC guidelines. *Geochimica et Cosmochimica Acta* **158**, 276–289.

LACOMBE, O., ANGELIER, J., BERGERAT, F. & LAURENT, P. 1990. Tectoniques superposees et perturbations de contrainte dans la zone transformante Rhin-Saone; apport de l'analyse des failles et des macles de la calcite. *Bulletin de la Société Géologique de France* **6**, 853–863.

LACOMBE, O., ANGELIER, J., LAURENT, PH., BERGERAT, F. & TOURNERET, CH. 1990. Joint analyses of calcite twins and fault slips as a key for deciphering polyphase tectonics: Burgundy as a case study. *Tectonophysics* **182**, 279–300.

LACOMBE, O., LAURENT, P. & ROCHER, M. 1996. Magnitude de la contrainte déviatorique pyrénéenne dans l'avant-pays nord-pyrénéen. *Comptes rendus de l'Académie des sciences. Série 2, Earth & planetary sciences.* **322**, 229–235.

LACOMBE, O. & MOUTHEREAU, F. 1999. Qu'est-ce que le front des orogènes ? L'exemple de l'orogène pyrénéen. *Comptes rendus de l'Académie des sciences. Série 2, Earth & planetary sciences.* **329**, 889–896.

LACOMBE, O. & OBERT, D. 2000. Héritage structural et déformation de couverture : plissement et fracturation tertiaires dans l'Ouest du bassin de Paris. *Comptes Rendus de l'Académie des Sciences - Series IIA - Earth and Planetary Science* **330**, 793–798.

LAWSON, M., SHENTON, B.J., STOLPER, D.A., EILER, J.M., RASBURY, E.T., BECKER, T.P., PHILLIPS-LANDER, C.M., BUONO, A.S., BECKER, S.P., POTTORF, R., GRAY, G.G., YUREWICZ, D. & GOURNAY, J. 2018. Deciphering the diagenetic history of the El Abra Formation of eastern Mexico using reordered clumped isotope temperatures and U-Pb dating. *GSA Bulletin* **130**, 617–629.

LEFORT, A., LATHUILIÈRE, B., CARPENTIER, C. & HUAULT, V. 2011. Microfossil assemblages and relative sea-level fluctuations in a lagoon at the Oxfordian/Kimmeridgian boundary (Upper Jurassic) in the eastern part of the Paris Basin. *Facies* **57**, 649–662.

LE ROUX, J. 1980. La tectonique de l'aureole orientale du Bassin de Paris; ses relations

avec la sedimentation. *Bulletin de la Société Géologique de France* **22**, 655–662.

LETOUZEY, J. 1986. Cenozoic paleo-stress pattern in the Alpine Foreland and structural interpretation in a platform basin. *Tectonophysics* **132**, 215–231.

MACCHIAVELLI, C., VERGÉS, J., SCHETTINO, A., FERNÀNDEZ, M., TURCO, E., CASCIELLO, E., TORNE, M., PIERANTONI, P.P. & TUNINI, L. 2017. A New Southern North Atlantic Isochron Map: Insights Into the Drift of the Iberian Plate Since the Late Cretaceous: Iberian Plate Kinematics Since 83.5 Ma. *Journal of Geophysical Research: Solid Earth* **122**, 9603–9626.

MALFILATRE, C. 2012. Mise au point d'une méthodologie analytique d'identification des pierres naturelles de construction. PhD Thesis, Université de Rennes. Published thesis.

MALFILATRE, C., BOULVAIS, P., DABARD, M.-P., BOURQUIN, S., HALLOT, E., PALLIX, D. & GAPAIS, D. 2012. Petrographical and geochemical characterization of Comblanchien limestone (Bourgogne, France): A fingerprint of the building stone provenance. *Comptes Rendus Geoscience* **344**, 14–24.

MANGENOT, X., GASPARRINI, M., GERDES, A., BONIFACIE, M. & ROUCHON, V. 2018. An emerging thermochronometer for carbonate-bearing rocks: $\Delta 47$ /(U-Pb). *Geology* **46**, 1067–1070.

MAZUREK, M., DAVIS, D.W., MADRITSCH, H., RUFER, D., VILLA, I.M., SUTCLIFFE, C.N., DE HALLER, A. & TRABER, D. 2018. Veins in clay-rich aquitards as records of deformation and fluid-flow events in northern Switzerland. *Applied Geochemistry* **95**, 57–70.

MOUTHEREAU, F., ANGRAND, P., JOURDON, A., TERNOIS, S., FILLON, C., CALASSOU, S., CHEVROT, S., FORD, M., JOLIVET, L., MANATSCHAL, G., MASINI, E., THINON, I., VIDAL, O. & BAUDIN, T. 2021. Cenozoic mountain building and topographic evolution in Western Europe: impact of billions of years of lithosphere evolution and plate kinematics (eds. O. Lacombe, S. Tavani, A. Teixell, D. Pedreira, & S. Calassou).

BSGF - Earth Sciences Bulletin **192**, 56.

NURIEL, P., WEINBERGER, R., KYLANDER-CLARK, A.R.C., HACKER, B.R. & CRADDOCK, J.P. 2017. The onset of the Dead Sea transform based on calcite age-strain analyses. *Geology* **45**, 587–590.

OLIVIER, N., CARPENTIER, C., MARTIN-GARIN, B., LATHUILIÈRE, B., GAILLARD, C., FERRY, S., HANTZPERGUE, P. & GEISTER, J. 2004. Coral-microbialite reefs in pure carbonate versus mixed carbonate-siliciclastic depositional environments: the example of the Pagny-sur-Meuse section (Upper Jurassic, northeastern France). *Facies* **50**, 229–255.

O'NEIL, J.R., CLAYTON, R.N. & MAYEDA, T.K. 1996. Oxygen isotope fractionation in divalent metal carbonates. *Journal of Chemical Physics* **51**, 5547–5557.

PAGEL, M., BONIFACIE, M., SCHNEIDER, D.A., GAUTHERON, C., BRIGAUD, B., CALMELS, D., CROS, A., SAINT-BEZAR, B., LANDREIN, P., SUTCLIFFE, C., DAVIS, D. & CHADUTEAU, C. 2018. Improving paleohydrological and diagenetic reconstructions in calcite veins and breccia of a sedimentary basin by combining Δ_{47} temperature, δ^{18}Owater and U-Pb age. *Chemical Geology* **481**, 1–17.

PARIZOT, O., MISSENARD, Y., HAURINE, F., BLAISE, T., BARBARAND, J., BENEDICTO, A. & SARDA, P. 2021. When did the Pyrenean shortening end? Insight from U–Pb geochronology of syn-faulting calcite (Corbières area, France). *Terra Nova* **33**, 551–559.

PARIZOT, O., MISSENARD, Y., BARBARAND, J., BLAISE, T., BENEDICTO, A., HAURINE, F. & SARDA, P. 2022. How sensitive are intraplate inherited structures? Insight from the Cévennes Fault System (Languedoc, SE France). *Geological Magazine*, 1–13.

PARRISH, R.R., PARRISH, C.M. & LASALLE, S. 2018. Vein calcite dating reveals Pyrenean orogen as cause of Paleogene deformation in southern England. *Journal of the Geological Society* **175**, 425–442.

PATON, C., HELLSTROM, J., PAUL, B., WOODHEAD, J. & HERGT, J. 2011. Iolite: Freeware for the visualisation and processing of mass spectrometric data. *Journal of Analytical Atomic Spectrometry* **26**, 2508.

PISAPIA, C., DESCHAMPS, P., BATTANI, A., BUSCHAERT, S., GUIHOU, A., HAMELIN, B. & BRULHET, J. 2018a. U/Pb dating of geodic calcite: new insights on Western Europe major tectonic events and associated diagenetic fluids. *Journal of the Geological Society* **175**, 60–70.

RING, U. & GERDES, A. 2016. Kinematics of the Alpenrhein-Bodensee graben system in the Central Alps: Oligocene/Miocene transtension due to formation of the Western Alps arc: Alpenrhein-Bodensee graben system. *Tectonics* **35**, 1367–1391.

ROBERTS, N.M.W., RASBURY, E.T., PARRISH, R.R., SMITH, C.J., HORSTWOOD, M.S.A. & CONDON, D.J. 2017. A calcite reference material for LA-ICP-MS U-Pb geochronology. *Geochemistry, Geophysics, Geosystems* **18**, 2807–2814.

ROBERTS, N.M.W., LEE, J.K., HOLDSWORTH, R.E., JEANS, C., FARRANT, A.R. & HASLAM, R. 2020. Near-surface Palaeocene fluid flow, mineralisation and faulting at Flamborough Head, UK: new field observations and U–Pb calcite dating constraints. *Solid Earth* **11**, 1931–1945.

ROBERTS, N.M.W. & HOLDSWORTH, R.E. 2022. Timescales of faulting through calcite geochronology: A review. *Journal of Structural Geology* **158**, 104578.

ROCHER, M., CUSHING, M., LEMEILLE, F., LOZAC'H, Y. & ANGELIER, J. 2004. Intraplate paleostresses reconstructed with calcite twinning and faulting: improved method and application to the eastern Paris Basin (Lorraine, France). *Tectonophysics* **387**, 1–21.

SIBSON, H, 1994. Crustal stress, faulting and fluid flow. In: Parnell, J. (Ed.), Geofluids: Origin, Migration and Evolution of Fluids in Sedimentary Basins, vol. 78. Geological Society, London, pp. 69–84 (Special Publication).

SMERAGLIA, L., LOOSER, N., FABBRI, O., CHOULET, F., GUILLONG, M. & BERNASCONI, S.M. 2021. U–Pb dating of middle Eocene–Pliocene multiple tectonic pulses in the Alpine foreland. *Solid Earth* **12**, 2539–2551.

SUN, X., GOMEZ-RIVAS E., CRUSET, D., ALCALDE, J., MUÑOZ-LOPEZ, D., CANTARERO, I.,MARTIN-MARTIN, J.D., JOHN, C.M., TRAVÉ A. 2022. Origin and distribution of calcite cements in a folded fluvial succession: The Puig-reig anticline (south-eastern Pyrenees). *Sedimentology*

SUTCLIFFE, C.N., THIBODEAU, A.M., DAVIS, D.W., AL-AASM, I., PARMENTER, A., ZAJACZ, Z. & JENSEN, M. 2020. Hydrochronology of a proposed deep geological repository for low- and intermediate-level nuclear waste in southern Ontario from U–Pb dating of secondary minerals: response to Alleghanian events. *Canadian Journal of Earth Sciences* **57**, 494–505.

SWART, P.K., BURNS, S.J. & LEDER, J.J. 1991. Fractionation of the stable isotopes of oxygen and carbon in carbon dioxide during the reaction of calcite with phosphoric acid as a function of temperature and technique. *Chemical Geology: Isotope Geoscience section* **86**, 89–96.

VANDEGINSTE, V., SWENNEN, R., ALLAEYS, M., ELLAM, R.M., OSADETZ, K. & ROURE, F. 2012. Challenges of structural diagenesis in foreland fold-and-thrust belts: A case study on paleofluid flow in the Canadian Rocky Mountains West of Calgary. *Marine and Petroleum Geology* **35**, 235–251.

VERMEESCH, P. 2018. IsoplotR: A free and open toolbox for geochronology. *Geoscience Frontiers* **9**, 1479–1493.

VILLEMIN, T. 1986. La chronologie des événements tectoniques dans le Nord-Est de la France et le Sud-Ouest de l'Allemagne du Permien à l'Actuel. *Comptes-Rendus de l'Académie des Sciences de Paris* **303**, 1685–1690.

VINCENT, B., EMMANUEL, L., HOUEL, P. & LOREAU, J.-P. 2007. Geodynamic control on carbonate diagenesis: Petrographic and isotopic investigation of the Upper

Jurassic formations of the Paris Basin (France). *Sedimentary Geology* **197**, 267–289.

WOODHEAD, J.D., HORSTWOOD, M.S.A. & COTTLE, P. 2007. 2016. Advances in Isotope Ratio Determination by LA–ICP–MS. *Elements* **12**, 317–322.

ZIEGLER, P.A. 1987. Late Cretaceous and Cenozoic intra-plate compressional deformations in the Alpine foreland—a geodynamic model. *Tectonophysics* **137**, 389–420.

ZIEGLER, P.A. & DÈZES, P. 2007. Cenozoic uplift of Variscan Massifs in the Alpine foreland: Timing and controlling mechanisms. *Global and Planetary Change* **58**, 237–269.

Samples	Outcrop locality or well	Stratigraphic age	Sedimentary formation or member	Nature	U-Pb age	2 S.E. abs.	2 S.E. %
PPA1073	Andra URL well	Upper Oxfordian	*Calcaires crayeux de Gudmont*	tension gash	50.4	2.4	4.7
SR6a	Sarazinière	Upper Oxfordian	*Oolithe de Lamothe*	tension gash N50°	58.9	1.8	3.0
SR6b				tension gash N150°	18.7	1.0	5.6
SR6c				Intergranular cement	57.7	2.6	4.5
LEU1-1	Leurville	Upper Oxfordian	*Oolithe de Saucourt*	Hydraulic breccia	27.0	1.1	4.2
LEU-2				Hydraulic breccia	22.2	1.2	5.5
A00607c	A901 - Montcornet	Upper Oxfordian	unknown	tension gash	47.3	6.4	13.4

	well						
SOR6 ab	Sorcy-Saint-Martin	Middle Oxfordian	*Craie de Sorcy*	tension gash	47.7	1.7	3.6
SOR6 c				tension gash	44.7	1.6	3.5
MXV7	Maxey-sur-Vaise	Middle Oxfordian	*Calcaires crayeux de Maxey*	tension gash N20°	48.0	3.5	7.3
MXV9 a				tension gash N175°	27.4	2.8	10.3
VCLD	Vaucouleurs	Middle Oxfordian	*Calcaires crayeux de Maxey*	tension gash N10°	43.2	1.4	3.3
DGS M29-1	Dugny-sur-Meuse	Middle Oxfordian	*Calcaires crayeux de Maxey*	tension gash N170°	31.6	2.9	9.2
DGS M29-2a		Middle Oxfordian	*Calcaires crayeux de Maxey*	tension gash N170°	32.0	1.5	4.5
DGS M29-2b				Intergranular cement	30.6	7.0	22.8
DGS M7a		Middle Oxfordian	*Calcaires crayeux de Maxey*	Vug	33.8	2.5	7.4
DGS M7b				Vug	39.0	1.7	4.4
DGS M7c				tension gash N40°	32.4	7.6	23.5
VOI3b	Void-Vacon	Middle Oxfordian	*Calcaires coralliens d'Euville*	tension gash	37.0	1.7	4.7
25209	Andra URL well	Middle Oxfordian	*Calcaires crayeux de Maxey*	tension gash	34.9	1.3	3.8
25229	Andra URL well	Middle Oxfordian	*Calcaires coralliens d'Euville*	Vug	33.2	2.2	6.7

25232 B a	Andra URL well	Middle Oxfordian	*Calcaires coralliens d'Euville*	tension gash	34.5	2.0	5.9
A901-22a	A901 - Montcornet well	Upper Bathonian	unknown	tension gash	92.9	10.3	11.1
A901-22c				tension gash	68.4	4.0	5.9
A901-22e				Intergranular cement	100.9	22.7	22.5
433-43240	EST433 well	Middle to Upper Bathonian	*Calcaires de Chaumont*	tension gash	33.0	5.5	16.6
BAZX 90 a	Bazoilles-sur-Meuse	Lower Bathonian	*Calcaires compacts de Neuchateau*	tension gash N10°	48.5	3.0	6.1
REM3-2	Removille	Upper Bajocian	*Calcaire du Bâlin/Oolithe miliaire inf*	tension gash	31.7	3.8	11.9
REM1				tension gash	42.1	2.7	6.3
OT-1-2	Ottange	Lower Bajocian	*Calcaire à polypiers inf*	Vug	40.8	2.2	5.4
SOM1-1	Sommerécourt	Lower Bajocian	*Calcaire à polypiers inf*	tension gash + Vug	42.5	3.9	9.1
SOM1-2				tension gash + Vug	40.9	1.7	4.2

Table 1. Samples description and associated calcite U-Pb geochronology data.

Samples	Stratigraphic	Nature	$\delta^{18}O_{‰V}$	$\delta^{13}C_{‰V}$	$\delta^{18}O_{‰V\text{-}PDB}$	$\delta^{13}C_{‰V\text{-}PDB}$	$T(\Delta_{47})$ mean	$T(\Delta_{47})$ error	$\delta^{18}O_{‰V\text{-}SMOW}$

	age		-PDB	-PDB	(clumped)	(clumped)	(°C)	(°C)	water
SR6b	Upper Oxfordian	tension gash			–7.5	2.7	27	3	–4.6
LEU1-1	Upper Oxfordian	Hydraulic breccia	–10.5	2.8					
LEU-2	Upper Oxfordian	Hydraulic breccia	–8.8	1.7					
SOR 6ab	Middle Oxfordian	tension gash	–7.0	3.2					
VCLD	Middle Oxfordian	tension gash	–7.7	3.4	–7.8	3.3	37	2	–2.9
VOI3b	Middle Oxfordian	tension gash	–7.1	3.1					
25209	Middle Oxfordian	tension gash	–8.4	2.9	–8.6	2.9	41	1	–2.9
25229	Middle Oxfordian	Vug	–9.0	2.9	–8.9	2.7	42	2	–3.1
A901-22a	Upper Bathonian	tension gash	–7.9	1.1					
BAZX 90 a	Lower Bathonian	tension gash	–10.5	1.4	–10.3	1.4	53	5	–2.6
REM 1	Upper Bajocia	tension gash	–10.3	1.5					

	n								
SOM 1-1	Lower Bajocian	tension gash + Vug	–9.1	2.0					

Table 2. Oxygen and carbon stable isotope composition and clumped isotope thermometry.

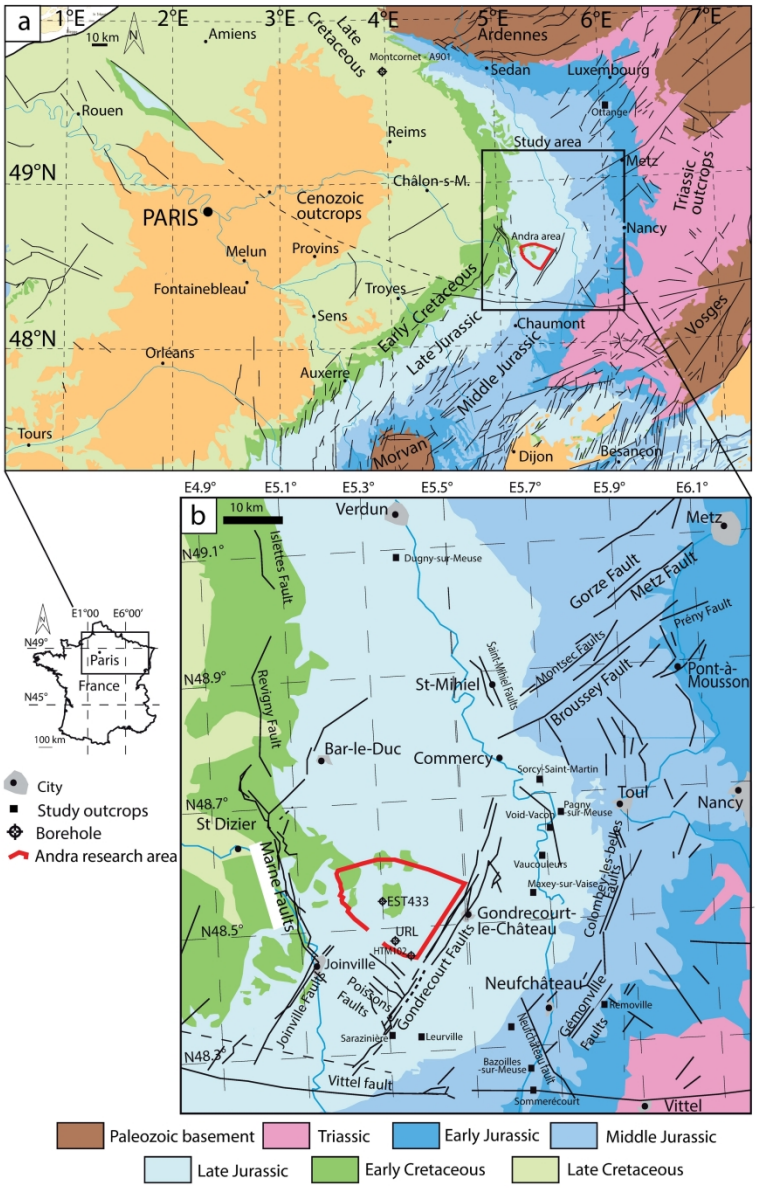

Figure 1. Geological map of the eastern Paris Basin (a), with a detailed view of the major structures in the studied area(b). Outcrop and quarries sample locations are indicated by black squares.

209x323mm (300 x 300 DPI)

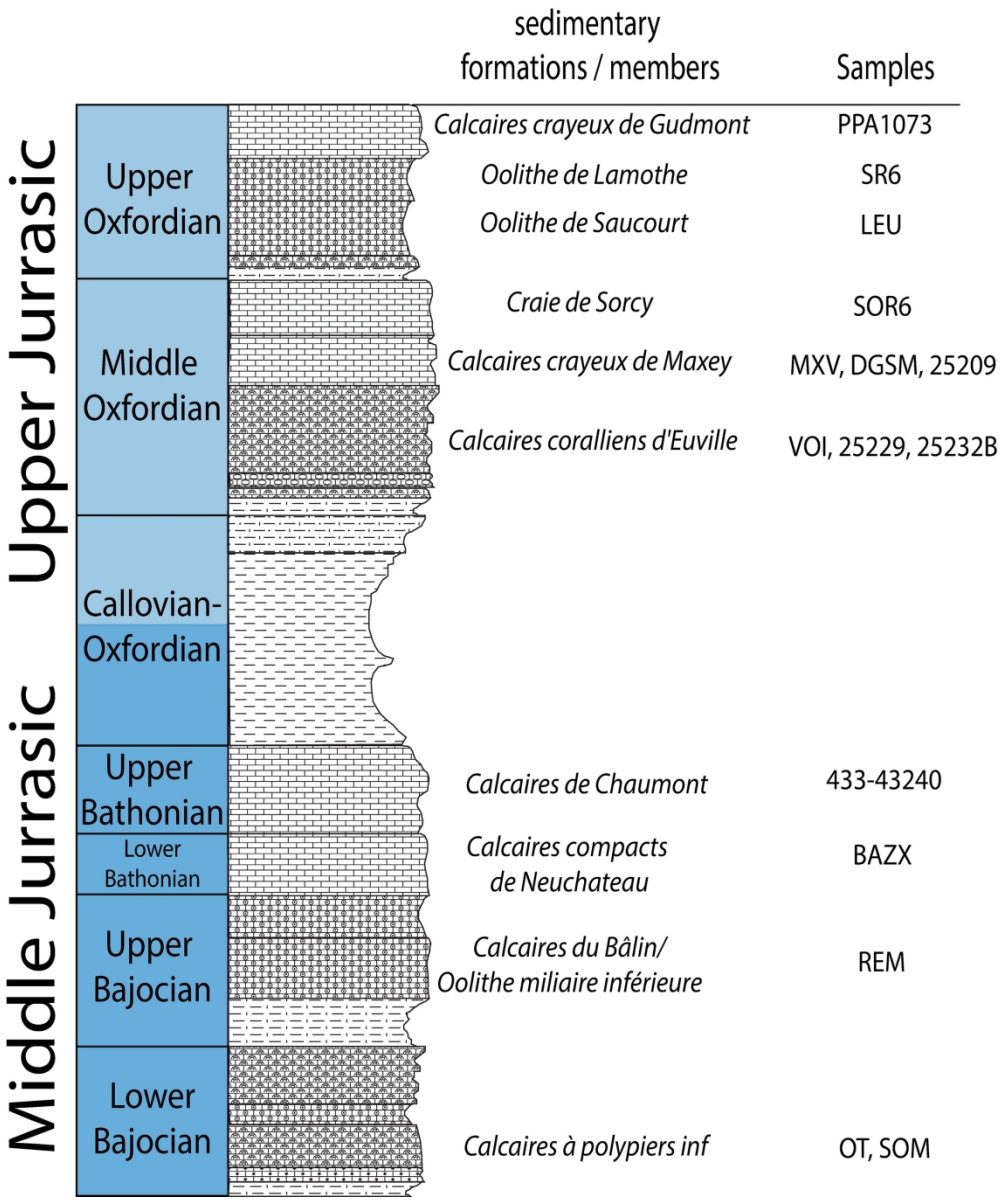

Figure 2. Simplified lithostratigraphic section in the eastern Paris Basin, showing the position of samples within the stratigraphic formations or members.

203x242mm (300 x 300 DPI)

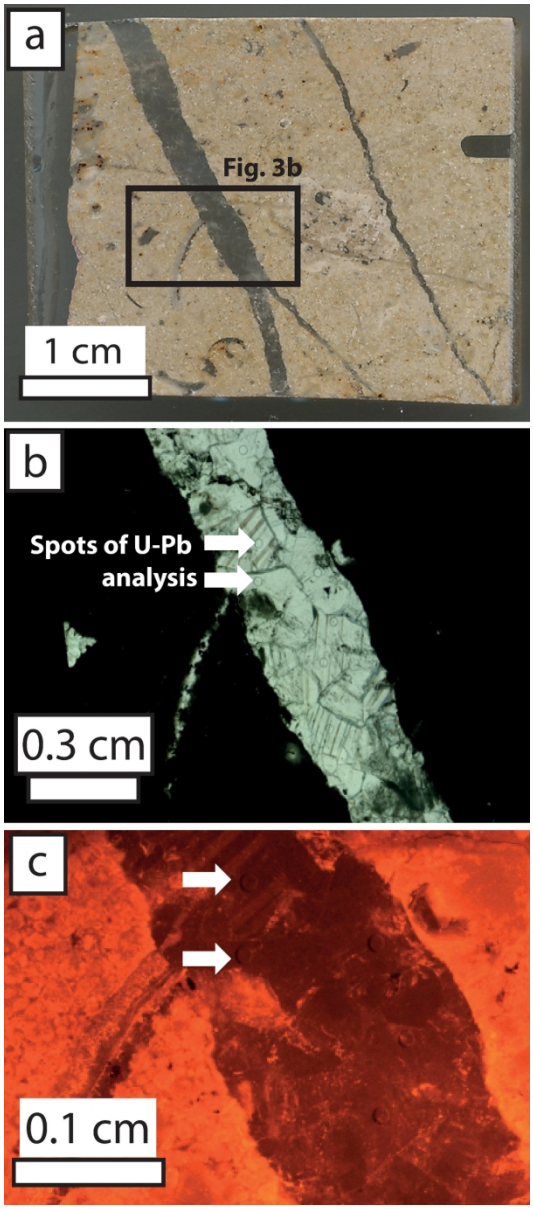

Figure 3. Example of sub-parallel tension gashes affecting a wackestone (a) sampled at Bazoilles-sur-Meuse (sample BAZX90a) in transmitted light (b) and cathodoluminescence microscopy (c). Ablation craters (150 µm in diameter) are visible in (b) and (c) (white arrows).

96x219mm (300 x 300 DPI)

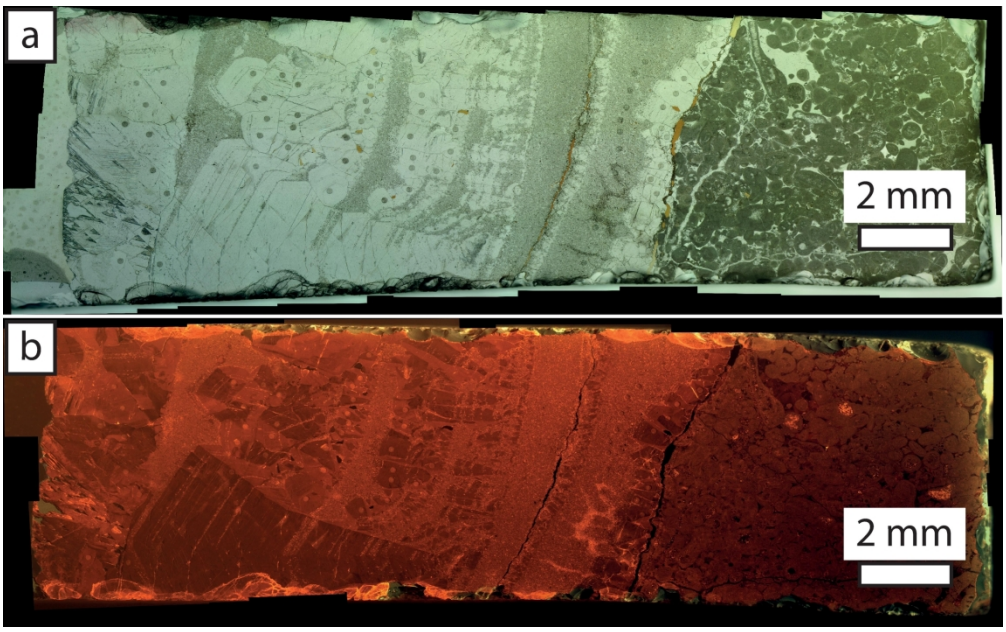

Figure 4. Hydraulic breccia developed in the oolithe de Saucourt Formation (sample LEU-2) in transmitted light (a) and cathodoluminescence microscopy (b). Ablation craters (150 µm in diameter) are visible.

205x127mm (300 x 300 DPI)

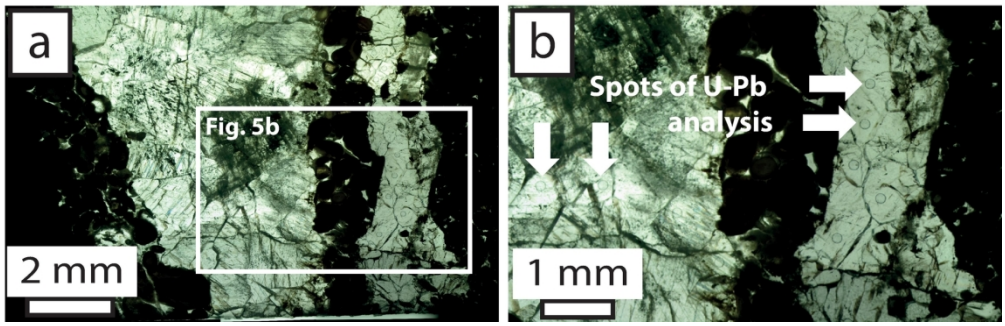

Figure 5. Tension gash in the oolithe miliaire Formation sampled at Removille (sample REM1) observed in transmitted light. The white square in photomicrograph (a) corresponds to the magnification in (b). This sample illustrates the impurities contained in some calcite cements. Ablation craters (150 µm in diameter) are visible (white arrows) and located, when possible, in the most limpid parts of the crystals.

167x61mm (300 x 300 DPI)

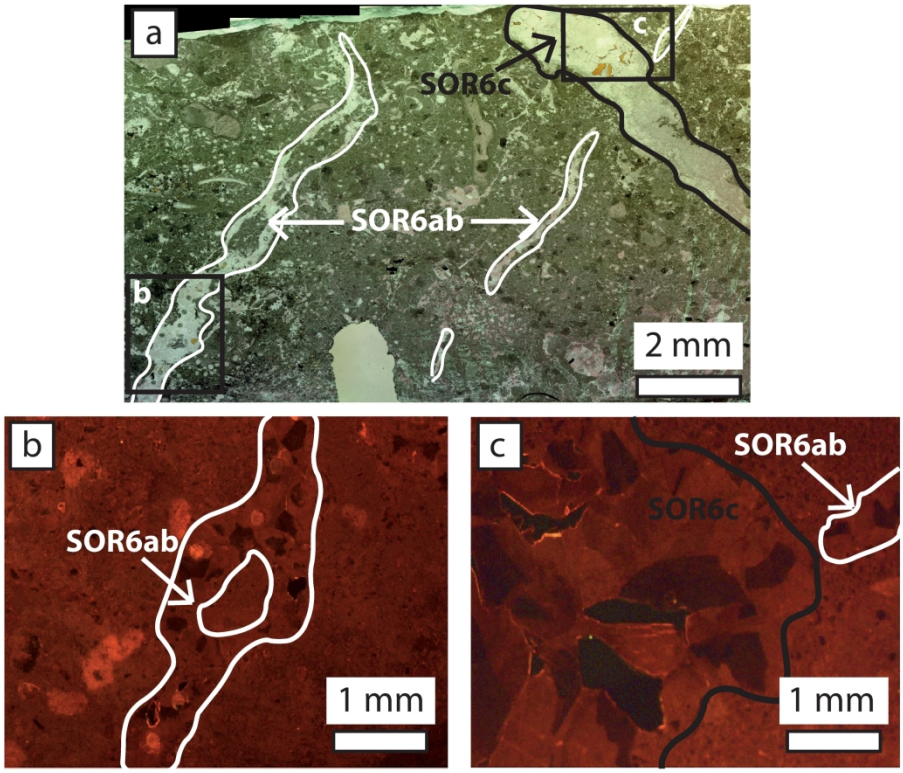

Figure 6. Tension gashes developed in sample SOR6 (Sorcy-Saint-Martin locality). The relative chronology between the fractures encircled in white (SOR6ab) and in black (SOR6c) is unclear, because no clear cross-cutting relationship is visible. Moreover, both tension gashes population is filled by blocky calcite displaying comparable cathodoluminescence.

230x213mm (300 x 300 DPI)

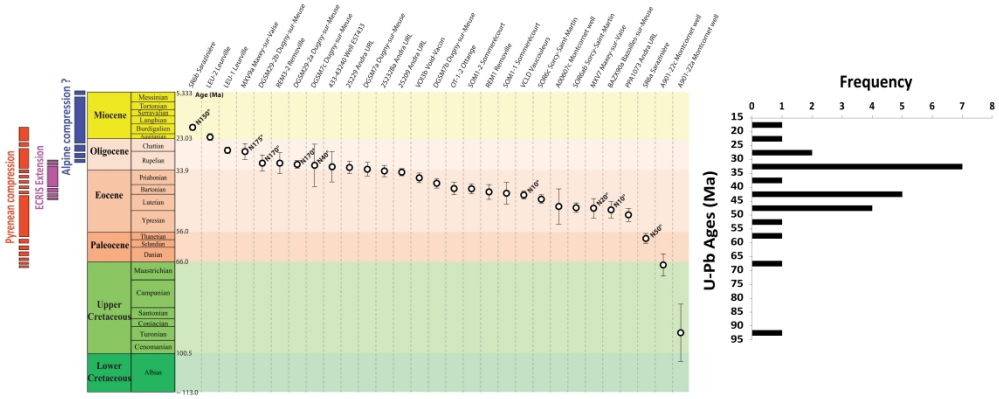

Figure 7. Compilation of calcite U-Pb ages in tension gashes and hydraulic breccias. In the histogram, data are plotted without considering the corresponding age uncertainties.

748x438mm (600 x 600 DPI)

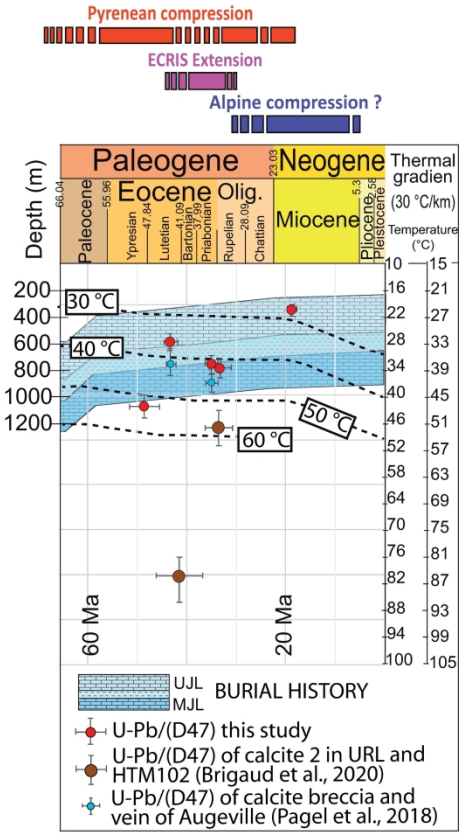

Figure 8. Calcite U-Pb age as a function of crystallization temperature determined from Δ47 thermometry.

209x328mm (300 x 300 DPI)

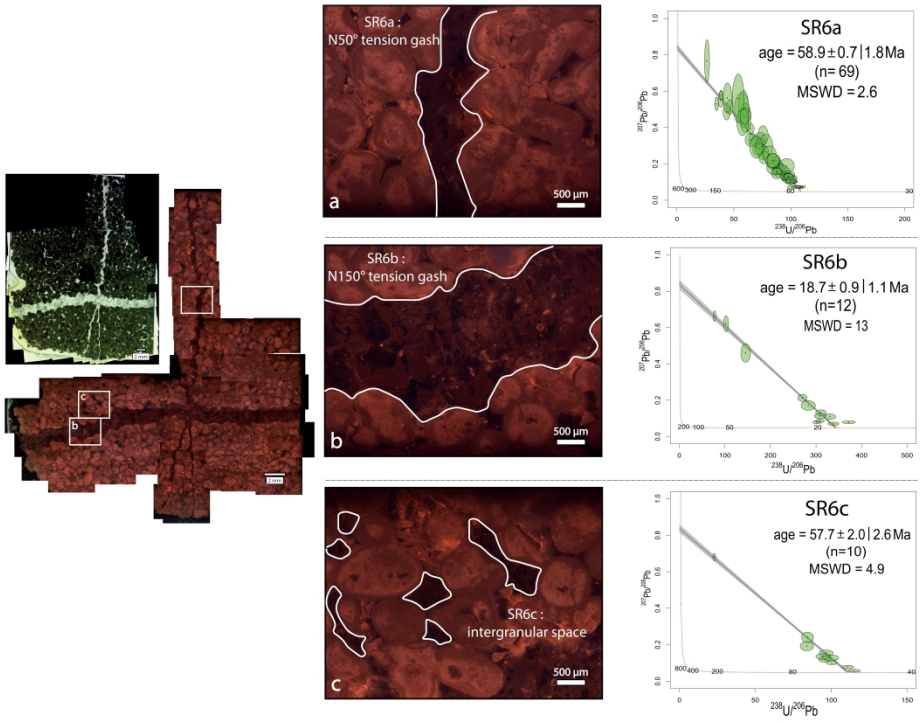

Figure 9. Calcite U-Pb ages determined in the SR6 sample (Sarazinière quarry, oolithe de Lamothe Formation, Upper Oxfordian).

1137x1119mm (600 x 600 DPI)